Int j simul model 21 (2022) 4, 639-650
Original scientific paper

AN ANFIS-MECHANISTIC SIMULATOR OF TOOL LOADS IN BALL-END MILLING OF LAYERED METAL MATERIALS

Zuperl, U.[*]; Kovacic, M.[**,***] & Brezocnik, M.[*]
[*] University of Maribor, Faculty of Mechanical Engineering, Smetanova 17, 2000 Maribor, Slovenia
[**] Štore Steel, d.o.o., Železarska cesta 3, 3220 Štore, Slovenia
[***] University of Ljubljana, Faculty of Mechanical Engineering, Aškerčeva cesta 6, 1000 Ljubljana
E-Mail: uros.zuperl@um.si

Abstract
This article presents a universal simulator of instantaneous loads on the cutting edges of ball-end mills for the processing of layered metal materials. The ANFIS-mechanistic simulator of cutting edge loads is designed for all typical geometries of ball-end mills and for layered materials with different machinability of individual layers. Two ANFIS (Adaptive Neuro Fuzzy Inference System) models are included in the simulator, which, based on the instantaneous radial thickness of the chip and the geometry of the spherical part of the ball-end mill, predict the material coefficients for the material layers. Comparison of the predicted tool loads with experimental data shows that the simulator accurately predicts the direction and magnitude of the instantaneous loads of the ball-end mill cutting edges when milling 3-layer metal material with different machinability of individual layers. The largest observed deviation of simulated load magnitudes for all verification machining tests is 21.7 %.
(Received in August 2022, accepted in October 2022. This paper was with the authors 1 month for 2 revisions.)

Key Words: Ball-End Milling, Layered Metal Material, Cutting Edge Loads, Coefficients of Material, ANFIS-Mechanistic Simulator

1. INTRODUCTION

New cutting tools enable reorganization of machining operations in production of components and appropriate productivity improvement [1]. The loads on cutting tools when processing thin-walled products made of advanced layered metal materials are exceptional. Knowing the loads on the tool cutting edges is important to choose the process parameters that result in longer tool life and minimal machining errors [2]. When designing new products, there is an increasing emphasis on aesthetics. Due to that requirement, the component shapes of the forming tools in the tool industry are becoming more complex. To produce complex sculpted pieces, the ball-end milling process is the only effective choice in today's toolmaking practice. The process of ball-end milling of spherical surfaces or sculptured products is extremely demanding for the following reasons. The first reason is the extremely complex cutting geometry of the tool and the constantly changing geometry of the resulting chip. The second reason is the modern and very difficult to process materials from which the components in the tool industry are made of. These are usually advanced layered metal materials that have a soft base onto which multiple metal layers with exceptional anti-wear and temperature-resistant properties are gradually deposited by a laser deposition processes. The laser engineered net shaping (LENS) process is often used in tool shops, where powdery metal is melted layer by layer with a laser into the final shape of the product. By adjusting the process parameters, the properties of the individual layers of the material and thus also the machinability of the multi-layer material are affected.

In the literature, several new research can be found that deal with the machinability of multi-layered metal materials. Li et al. [3] conducted a comprehensive review of the literature in the field of machinability of additively manufactured titanium alloys. Khanna et al. [4] have provided a precise overview of research dealing with the procedures of additively manufactured nickel and titanium alloys. Among the most important studies, it is worth highlighting Zhang

et al. [5], who identified problems with machinability in the post-processing of additively manufactured thick coatings. Altiparmak et al. [6] analysed the machinability of high-strength aluminium alloys that were manufactured using additive technologies. In the research [7], the machinability of Inconel 718 nickel-based alloy and 316L stainless steel was tested with ceramic and carbide mills. Periane et al. [8] studied face milling of additively and conventionally manufactured parts from Inconel 718. Ji et al. [9] analysed the machinability of Inconel 718 during the micro-milling process. In the research [10] studied the effect of cutting parameters during end milling on Inconel 625 parts manufactured by using the Laser Powder Bed Fusion process. Zhang et al. [11] studied the machinability of Ti6Al4V in high-speed dry milling with ceramic flute tools. They studied the machinability of additively manufactured Ti6Al4V with solid ceramic tools at high speed. The research [12] studied machinability and cutting forces in face milling of aluminium alloy 7075. Ming et al. [13] have reported that such materials have distinctly difficult machinability compared to metallic materials that are produced by conventional processes such as casting, forging, etc.

Due to the variable cutting geometry and the variable machinability of the material from layer to layer, the processing of such materials is extremely demanding. The difficulty is mainly manifested in machining errors. The most common causes of machining errors in ball-end milling are shock loads on the tool, which cause tool deflections and excessive tool wear. Therefore, precise knowledge of the tool loads is essential for the processing of sculptured products from layered materials without machining errors.

Many cutting force models for the ball-end milling processes have been published in the literature. The models that dominate are those that calculate the cutting forces based on the radial thickness of the undeformed chip and the coefficient of material. The simplest of them are the average cutting force models [14, 15]. These models provide information on the cutting force magnitude. The cutting force magnitude and direction are given by instantaneous force models, which calculate the force based on the instantaneous chip radial thickness. Several instantaneous cutting force models have been developed for the ball-end milling process [16-19]. Flexible models of forces were developed, which consider the deviations of the ball-end mill and the elasticity of the workpiece in the calculations [20]. The following is a presentation of the most important cutting force models in ball-end milling. Lee and Altintaş [21] developed a differential cutting force modelling technique for ball-end mills. In the research [22], the edge force has been modelled in the ball-end milling of inclined surfaces. Wang et al. [23] developed a cutting force model for five-axis ball-end milling. Tool wear and vibration were introduced into the model. Simulation analyses of the impact of adding controlled vibrations of different amplitudes and frequencies on the quality of processing can be studied in [24]. In the research [25], a model of cutting forces for 5-axis ball-end milling of sculptured surfaces has been presented. Jia et al. [26] introduced the material properties of the workpiece into a model for predicting cutting forces. In the study [27], the Deform 3D finite element analysis software was used to simulate the ball-end milling and to analyse the distribution patterns of milling forces. In research [28], a model of cutting forces and surface topography for the side milling process has been demonstrated. In the study [29], a mechanical model of cutting forces was developed by considering the trajectory of the cutting edge and the geometric error of the system. The practical prevalence of instantaneous models of tool cutting edge loads in industry limits the time-consuming determination of tangential and radial material coefficients [30]. Experimental determination of material coefficients for multi-layer metallic materials, where machinability varies from layer to layer, represents an additional challenge. Only a few studies dealing with the modelling of cutting forces in helical-end milling of composites could be found in the literature [31, 32]. He et al. [33] created a model of cutting forces for milling the carbon fibre-reinforced polymer (CFRP) composites, in which the specific cutting forces were calculated by considering the current chip thickness, fibre cutting angle and

cutting speed. More important is the research [34] on the modelling of instantaneous cutting forces in the end milling of curved carbon fibre reinforced polymer (CFRP) components in combination with the research [35] on the identification of vibrations with machine learning. To the best of our knowledge, there is no research that considers the different machinability of layers of laser-cladded metal material when modelling the instantaneous loads of a ball-end mill.

Therefore, this article presents a hybrid ANFIS-mechanistic simulator of instantaneous loads on the tool cutting edges for horizontal ball-end milling of layered metal materials, considering different machinability of individual layers. The simulator includes two ANFIS models for predicting the tangential and radial material coefficients of individual material layers. The simulator calculates the instantaneous directions and magnitudes of the cutting edge loads for all typical ball-end mill geometries.

The article is organized as follows. Section 2 presents a simulator of instantaneous loads on the tool cutting edges for the process of spherical shape milling of layered materials. Section 3 describes the mechanistic part of the simulator with a pseudocode for predicting the loads on the ball-end mill cutting edges. Section 4 presents experimental methodology for determining the tangential and radial coefficients of the material. The experimental part of the research with the equipment used is described in Section 5. Section 6 provides a comparison between the simulator and experimental results. Section 7 gives the concluding remarks.

2. SIMULATOR OF BALL-END MILL CUTTING EDGE LOADS

A universal ANFIS-mechanistic simulator of instantaneous cutting edge loads for shape milling of multilayer materials is described. The simulator is designed for all typical geometries of ball-end mills and for any layered materials. It is particularly effective in milling of layered materials with layers of different machinability. The inputs to the simulator are the cutting parameters, the radius of the ball-end mill, the cutting geometry of the tool and the geometry of the chip. To determine the loads of a ball-end mill with a mechanistic model, it is necessary to distribute the chip load over the active part of all flutes. Fig. 1 shows the shape of the chip and the radial thickness of the undeformed chip at the point of operation of the differential cutting disc D. The elementary load of the cutting disc is determined as the product of the coefficient of material and the chip cross-section. The coefficients of material are estimated with the ANFIS prediction system. Cutting data is used to build the ANFIS system. The radial thickness of the chip *d* at the location of the cutting disc D of the cutting edge is equal to the radial distance between the two largest vertical surfaces that form the chip. The sum of the elementary loads on all active cutting discs determines the total load of the ball-end mill.

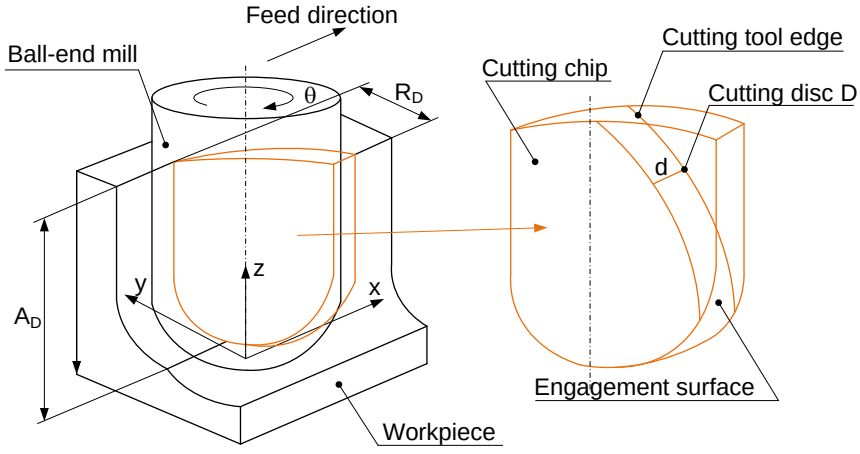

Figure 1: Chip form in ball-end milling.

3. ARCHITECTURE OF THE BALL-END MILL LOAD SIMULATOR

The tool cutting edge load simulator is designed for all typical geometries of ball-end mills and for layered materials with different machinability of individual layers. The simulator predicts directions and amplitudes of instantaneous tool load. To show the geometry of the cutting edge, the ball-end mill is divided into thin cutting discs along the tool axis. The diameter of the discs varies with the height of the mill from 0 to R, where R is the radius of the ball-end mill (Fig. 2). The radius r of the disc D at the height z is determined according to Eq. (1).

$$r(z) = \sqrt{z(2R - z)} \text{ for } 0 \leq z < R \tag{1}$$

The angular position of the disc D on the cutting edge j for a ball-end mill with N flutes is calculated according to:

$$\Theta_j(\theta, z) = \Theta - \frac{2\pi\,(j-1)}{N} - \frac{z \cdot \tan\beta}{R} \tag{2}$$

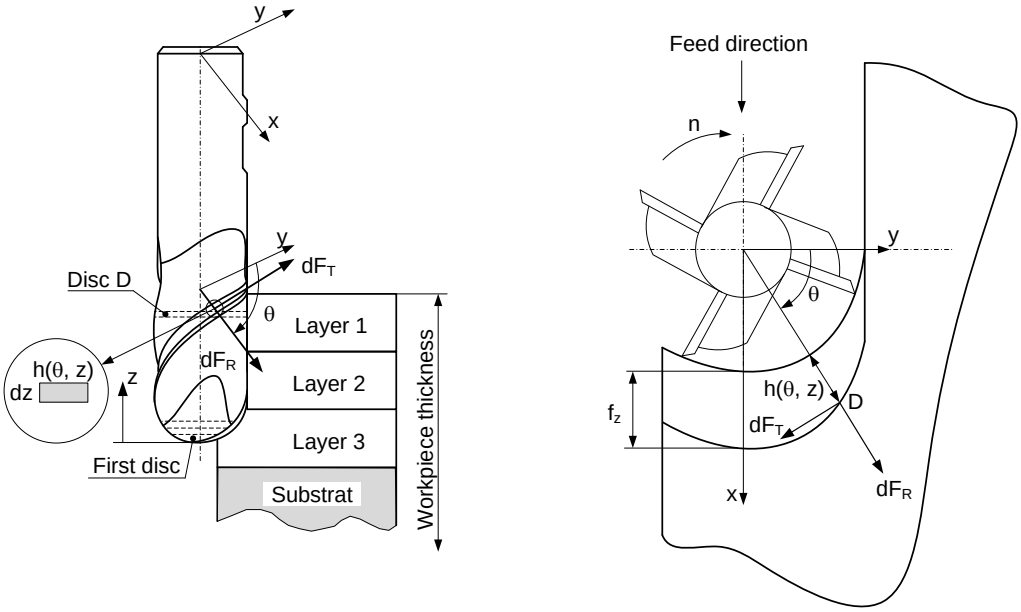

Figure 2: Ball-end mill with D cutting disc load and chip cross-section in horizontal milling of layered material.

In Eq. (2), the helix angle is designated as β and the angular position of the first flute as Θ. If the cutting speed is much higher than the feed speed of the tool, then the path of the tool tooth is circular. A simplified tool tooth path, the chip cross-section and the radial thickness of the undeformed chip are shown in Fig. 2. Radial thickness of undeformed chip $d(\Theta)$ on the cutting disc D when feeding in the horizontal plane and at the angle of rotation Θ is calculated according to the equation:

$$d(\Theta) \approx f_z \cdot \sin\Theta \tag{3}$$

where f_z is feed per tooth of the tool. The radial component of the cutting force dF_T and the tangential component of the cutting force dF_R of the loaded cutting disc D on the j^{th} cutting edge are shown in Fig. 2. The disc D is at a distance z from the tip of the tool. Both components of the cutting force on disc D are designated as:

$$dF_{Tj}(\Theta, z) = K_T(z) \cdot \left[d_j(\Theta, z)\right]^{0.8} \cdot dz \tag{4}$$

$$dF_{Rj}(\Theta, z) = K_R(z) \cdot \left[d_j(\Theta, z)\right]^{0.8} \cdot dz \tag{5}$$

where dz is the axial depth of the disc cut at height $z, d_j(\Theta, z)$ is the radial thickness of the undeformed chip K_T and K_R are coefficients of material.

Both coefficients of material depend on the position of the disk D on the ball part of the mill and on the machinability of each layer of the multilayer material. The two differential cutting forces on the disk are equal to the product of the coefficient of material and the radial thickness of the undeformed chip at the angle of tool rotation Θ.

The resulting instantaneous tool loads are equal to the sum of the differential tangential and radial cutting forces on all active tool discs. The resulting instantaneous loads are decomposed into the x-y plane by:

$$F_x(\Theta) = \int_{z=0}^{A_D} \left[\sum_{j=1}^{N} K_T(z) \cdot \left[d_j(\Theta, z)\right]^{0.8} \left[-cos\,\Theta_j\right] + K_R(z) \cdot \left[d_j(\Theta, z)\right]^{0.8} \left[-sin\,\Theta_j\right] \right] dz \quad (6)$$

$$F_y(\Theta) = \int_{z=0}^{A_D} \left[\sum_{j=1}^{N} K_T(z) \cdot \left[d_j(\Theta, z)\right]^{0.8} \left[sin\,\Theta_j\right] + K_R(z) \cdot \left[d_j(\Theta, z)\right]^{0.8} \left[-cos\,\Theta_j\right] \right] dz \quad (7)$$

In the equation, A_D designates the axial depth of cut.

Ball-end mill cutting edge load simulator pseudocode for layered materials is presented in Table I.

Table I: Ball-end mill cutting edge load simulator pseudocode.

Read_inputs	
Cutting parameters	F_z, n, A_D, R_D
Ball-end mill geometry	R, N, β
Specific cutting forces/layer	K_T, K_R
No. of cutting disc	k
No. of cutting flute	j
Write_outputs	
Cutting edge loads/cutting angle	$F_y(\Theta), F_x(\Theta)$
Calculation_variables	
Calculation of tool feed	f
Setting the cutting angle	$\Theta = 0$
If $\Theta \leq \Theta_{exit}$	Cutting angle integration $0 \leq \Theta \leq \Theta_{exit}$
Calculation of radial thickness of undeformed cutting chip	$d(\Theta)$
Set $F_x, F_y = 0; k = 1$	
If $k \leq K$	Integration loop from 0 to A_D
Determine cutting angle	Θ
Recall K_R and K_T	
Calculation of momentary forces	$dF_T(\Theta, z)$and $dF_C(\Theta, z)$
Transformation of cutting force in x-y direction	$dF_y(\Theta)$, $dF_x(\Theta)$
Determination of cumulative force	$F_x(\Theta)$ and $F_y(\Theta)$
next k	$k = k + 1$
Else	
$\Theta = \Theta + 2\,p\,n\,t/60; t$ (s)	
Resultant cutting force at Θ	$F(\Theta) = \sqrt{F_x(\Theta) + F_y(\Theta)}$
Print $F_y(\Theta), F_x(\Theta), F(\Theta)$	
else	
stop	
end	

4. DETERMINATION OF MATERIAL CONSTANTS

Layered metal materials are used in the research, whereby the material layers have different properties and machinability.

Great attention has been paid to the fact how to determine the material coefficients for individual layers of the multi-layer material. When calculating the tangential coefficient K_T of material layers and radial coefficient R_T of material layers it was necessary to consider the variable geometry of the spherical part of the ball-end mill in addition to the instantaneous radial thickness of the chip. It has been established that the magnitudes of the material coefficients also depend on the position of the cutting disc D of the tool in the z-axis. The diameters of the cutting discs and thus the cutting conditions change along the z-axis in the spherical part of the ball-end mill. Coefficient K_T and K_R change along the z-axis up to the height $z = R$. At height $z = R$, the tool radius is constant, so the material coefficients are also constant.

The material coefficient for a certain layer of layered material is experimentally determined as the ratio between the experimentally determined average measured component of the cutting forces and the average cross-section of the chip.

$$K_T(z) = \frac{F_{T\,av}}{\sum_{z=0}^{A_D} \sum_{\Theta=\Theta_{ent}}^{\Theta_{ex}} \left[\frac{[d(z,\Theta)]^{0.8}}{(\Theta_{ex} - \Theta_{ent}) \cdot \left(\frac{A_D}{dz}\right)} \cdot dz \right]} \tag{8}$$

$$K_R(z) = \frac{F_{R\,av}}{\sum_{z=0}^{A_D} \sum_{\Theta=\Theta_{ent}}^{\Theta_{ex}} \left[\frac{[d(z,\Theta)]^{0.8}}{(\Theta_{ex} - \Theta_{ent}) \cdot \left(\frac{A_D}{dz}\right)} \cdot dz \right]} \tag{9}$$

The procedure of experimental determination of the material coefficients starts with the measurement of the average cutting force $F_{x\,av}$ and $F_{y\,av}$ between the entry cutting angle Θ_{ent} and exit cutting angle Θ_{ex}. The transformation of the force $F_{x\,av}$ and $F_{y\,av}$ into the average tangential $F_{T\,av}$ and radial cutting force $F_{R\,av}$ follows.

The average differential cross-section of the chip is determined by the product of the differential chip height dz and the average radial thickness of the undeformed chip that occurs between the entry of the flute into the material and the exit of the flute from the material. By inserting the values in Eqs. (8) and (9), the tangential and radial coefficients of the material are determined.

The data for the calculation of the material tangential and radial coefficients were obtained by machining tests. During the experiments on the horizontal machining centre Heller BEA1, the material constants were calculated for each individual material layer. A ball-end mill of diameter 4 mm was used.

Machining tests were performed on 3 different layered metal workpieces with two levels of axial depth of milling, three levels of radial depth of milling, two spindle speeds and three levels of feed speed. The results of this study are discussed only for one radial depth of milling. The three workpieces were single-layered with different thickness and hardness of the cladded gradient layer.

The data obtained from the experiments were used to create two ANFIS predictive models of material coefficients. One-third of randomly selected data rows were used for model verification.

ANFIS models generalize tangential or radial coefficient of the material in relation to the cutting parameters and the thickness and hardness of the material layer.

The generated Fuzzy inference structure (FIS) of the models is shown in Fig. 3. FIS connects 6 inputs to one output with 20 logical decision rules.

The training of the ANFIS models was stopped after 150 iterations of hybrid learning.

A method 10-fold cross-validation is used to assess the accuracy of the constructed ANFIS models. The calculated average prediction error (APE) of the 10 models is used to evaluate the accuracy of the model in practice.

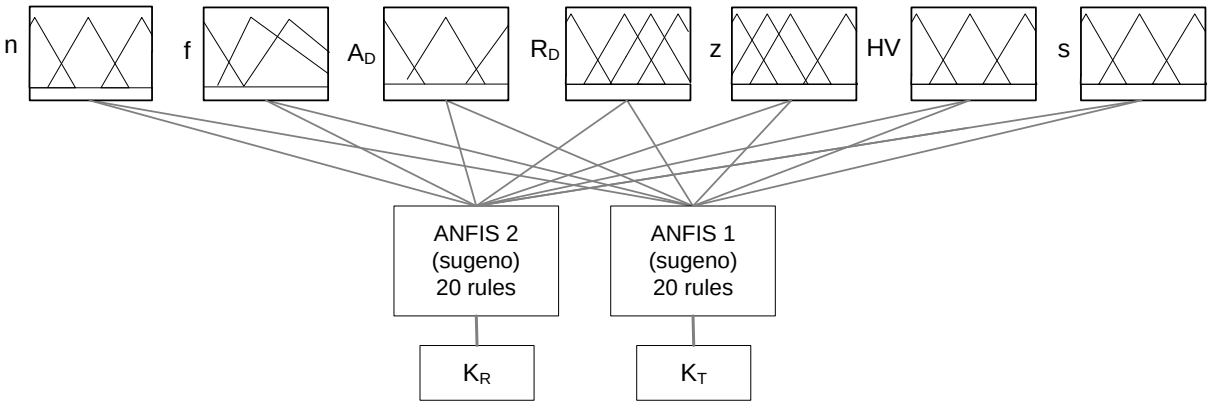

Figure 3: Linking FIS systems to predict material coefficients with model inputs and outputs.

5. EXPERIMENTAL TESTING EQUIPMENT

Machining experiments have been implemented to create ANFIS models of material coefficients and to verify the predictive capabilities of the instantaneous loads simulator of cutting edges for ball-end milling of multi-layer materials.

Experiments without the use of coolant are carried out on the Heler BEA 01 horizontal centre. Carbide ball-end mills with a radius of 4 mm, two cutting edges and a helix angle of 32.2° were used. The tool material is sintered tungsten carbide having a hardness of 1790 HV and TiAlN coating.

Four different workpieces were produced on Optomec LENS 850-R machine. The basic material of all workpieces is steel 20MnCr5. In one workpiece, 3 layers of stainless steel 904L of different thicknesses and hardnesses are applied to the base material (Fig. 1). The rest of the workpieces have a base of 20MnCr5 on which only one layer of 904L stainless steel is applied.

The thickness and hardness of the applied layer is different on each workpiece. All layers are made with 45 % overlapping. Layer hardness is determined by using a 7061 Zwick 3212 hardness tester, and layer thickness by Metallurgical Microscope Epiphot 300.

The instantaneous cutting load components F_x and F_y were measured by using a Kistler 9257A piezoelectric dynamometer and a Kistler Dual Mode charge amplifier. A low pass filter of 1.1 kHz cut-off frequency is used to eliminate noise. A sampling frequency of 1.8 kHz was selected for each channel. NI data acquisition board and LabVIEW software were used. Each cutting force measurement was repeated three times.

In the experiment, 2 levels of axial cutting depth were selected: $A_{D1} = 0.5$ mm, $A_{D2} = 0.9$ mm. Radial depth of cut R_D was set to 0.28. Three levels of spindle speed and tool feed are used: $n_1 = 3000$ min^{-1}, $n_2 = 3500$ min^{-1}, $n_3 = 3800$ min^{-1}; $f_1 = 180$ mm/min, $f_2 = 230$ mm/min, $f_3 = 280$ mm/min. Machining experiments with workpieces to create the ANFIS model of material coefficients and to verify the created simulator of instantaneous cutting edge loads are shown in Fig. 4.

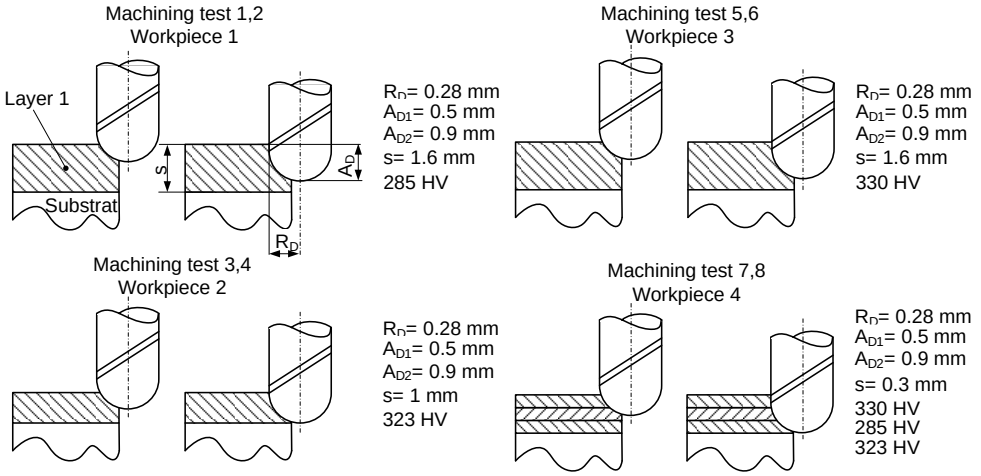

Figure 4: Machining tests with the structure of the workpieces to create the ANFIS model of the material coefficients and to verify the simulated instantaneous loads of the cutting edges.

6. RESULTS AND DISCUSSION

Experiments have shown that the coefficients of the material K_T and K_R decreases with height z. The change in the value of the tangential and radial coefficient of the material for Machining test 1 and 2 can be approximated by the following equations:

$$K_T = 2451 - 1376\frac{z^3}{R^3} + 450\frac{z^2}{R^2} - 4170\frac{z}{R};\ 0 \le z \le R \tag{10}$$

$$K_R = -54 - 2824\frac{z^3}{R^3} - 6360\frac{z^2}{R^2} + 4185\frac{z}{R};\ 0 \le z \le R \tag{11}$$

The values K_T and K_R predicted with ANFIS models with respect to height z are shown in Fig. 5. It can be seen from the graph in Fig. 5 that the predicted magnitudes of K_T and K_R are in good agreement with experimentally obtained magnitudes. The K_R value decreases monotonically with height. The K_T value first increases with height z, reaches an extreme, then begins to slowly decrease. In all machining tests, the K_T coefficient reaches its maximum value at a height equal to half the tool radius.

The average percentage error (*APE*) method was used to evaluate the accuracy of the ANFIS models. The results of the analysis of the models using the 10-fold cross-validation method show that the ANFIS model predicts K_T with a maximum error of 4.9 % and a confidence interval of 95 %. While the material coefficient K_R is predicted with a maximum error of 3.4 % and a confidence interval of 95 %.

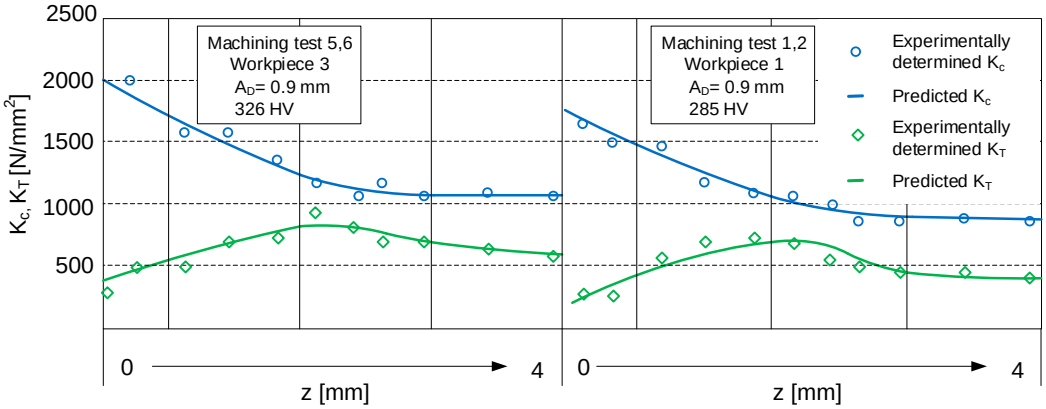

Figure 5: Matching of predicted magnitudes of K_T and K_R coefficients with experimentally obtained; $n = 3500$ min^{-1}, $f = 230$ mm/min.

The hybrid ANFIS-mechanistic simulator simulates instantaneous horizontal loads of cutting edges during ball-end milling of three-layer metal material. The chapter describes an example of a machining test (Machining test 8), which served to validate the cutting edge load simulator. Fig. 6 shows the simulated and experimental results for Machining test 8 with an axial depth of 9 mm. The lines on the graph show the directions and amplitudes of the instantaneous loads in relation to the rotation angle of the ball-end mill. The measured instantaneous tool loads are shown in the graph with solid lines.

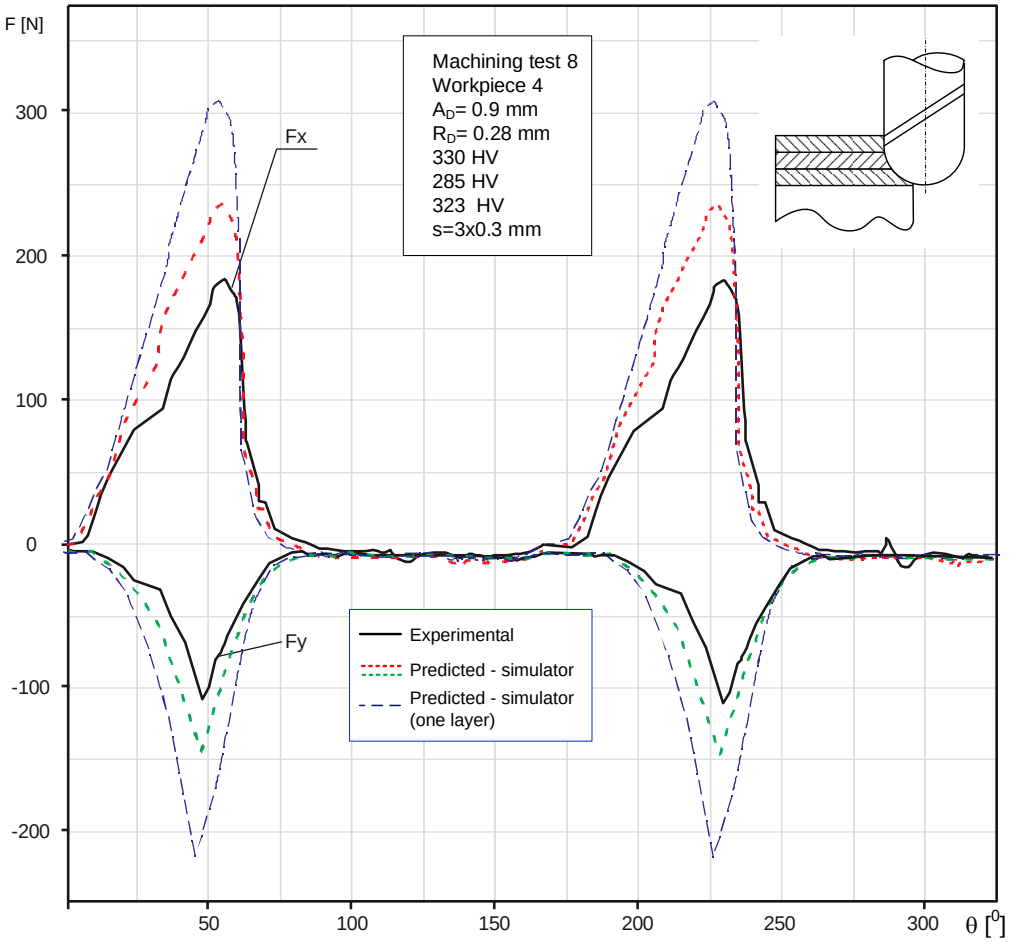

Figure 6: Simulated and experimental loads of a ball-end mill cutting edges in the machining of three-layer material; $n = 3800$ min^{-1}, $f = 280$ mm/min.

The graph shows two load shocks in the x- and y-axes, which is the result of using a tool with two flutes. Due to the new, unworn ball-end mill, the flow of loads on both flutes is symmetrical. The jump in cutting force with extreme occurs at the exit angle of the cut Θ_{ex}, where the instantaneous radial chip thickness is the maximum. A load jump of magnitude 180 N occurs at a cutting angle of 55°. The tendency of the load jump is to push the tool away from the machining surface, leading to a machining error. The shape and magnitude of the load is influenced by the thickness and hardness of the individual layers of the material. During the rotation of the tool, the cutting edge of the tool is in contact with three different processing layers of the material. The magnitudes of the loads are largest when processing the upper layer, mainly due to the highest hardness of this layer and the maximum speed of the cutting edge at this height. The results of the simulator, which takes into account the different machinability of individual layers of material, are marked with dashed lines. The time course of the predicted loads agrees well with the experimental course, while deviations occur in the magnitudes of the loads. The model overestimates the magnitudes of the loads. An even greater overestimation of

load magnitudes is observed in the results of the simulator, which treats three layers as one layer and when doing calculation, considers the most unfavourable machinability of the layer (layer 1 with a hardness of 320 HV). The results are represented by a dashed thin line. Inappropriately calculated material coefficients for the remaining two layers are the cause of the difference in load amplitudes. From the results in Fig. 6, it can be seen that the simulator adequately predicts the instantaneous loads of the ball-end mill when machining layered metal materials. The values of the predicted and measured load magnitudes differ from 4 % to 21.7 % for the load in the x-axis. Load deviations in the y-axis are from 3.6 % to 17.8 %.

7. CONCLUSION

This article presents a new approach to simulating the loads on the cutting edges of tools during the horizontal milling of layered metal materials with variable layer machinability. The hybrid ANFIS-mechanistic simulator consists of two parts. The mechanistic part of the simulator calculates the instantaneous direction and magnitude of the flute load based on the instantaneous radial thickness of the undeformed chip. The calculation considers the machinability of all material layers that are in contact with the tool flute. To determine the material constants of individual material layers, two ANFIS models have been created, which represent the second part of the simulator. The following conclusions can be drawn from the machining experiments for the verification of the simulator.

The time course of the predicted loads agrees well with the experimentally obtained course; deviations occur in the magnitudes of the loads. The simulator overestimates the magnitude of the loads at the exit cutting angle. A significant overestimation of load magnitudes has been noted in the results of the simulator, which treats three layers as one layer and takes the most unfavourable machinability of the layer for the calculation. The values of the predicted and measured load magnitudes differ from 4 % to 21.7 % for the load in the x-axis. Load deviations in the y-axis are from 3.6 % to 17.8 %. The results of the analysis of the ANFIS models using the 10-fold cross-validation method show that the ANFIS models predict the material constants with a maximum error of 4.9 % with a confidence interval of 95 %.

The goal of further research is to include the vertical component of the tool feed in the simulator, to improve the calculation of the radial chip thickness for sculptured surfaces and to increase the database for training ANFIS models of material coefficients.

REFERENCES

[1] Da Silva, J. C.; da Silva, F. J. G.; Campilho, R. D. S. G.; de Sa, J. C. V.; Ferreira, L. C. R. N. P. (2021). A model for productivity improvement on machining of components for stamping dies, *International Journal of Industrial Engineering and Management*, Vol. 12, No. 2, 85-101, doi:10.24867/IJIEM-2021-2-279

[2] Antić, A.; Zeljković, M.; Ungureanu, N.; Kuric, I. (2018). Tool condition monitoring system based on a texture descriptors, *International Journal of Industrial Engineering and Management*, Vol. 9, No. 3, 167-175, doi:10.24867/IJIEM-2018-3-167

[3] Li, G.; Chandra, S.; Rahman Rashid, R. A.; Palanisamy, S.; Ding, S. (2022). Machinability of additively manufactured titanium alloys: a comprehensive review, *Journal of Manufacturing Processes*, Vol. 75, 72-99, doi:10.1016/j.jmapro.2022.01.007

[4] Khanna, N.; Zadafiya, K.; Patel, T.; Kaynak, Y.; Rahman Rashid, R. A.; Vafadar, A. (2021). Review on machining of additively manufactured nickel and titanium alloys, *Journal of Materials Research and Technology*, Vol. 15, 3192-3221, doi:10.1016/j.jmrt.2021.09.088

[5] Zhang, P.; Liu, Z.; Du, J.; Su, G.; Zhang, J.; Xu, C. (2020). On machinability and surface integrity in subsequent machining of additively-manufactured thick coatings: a review, *Journal of Manufacturing Processes*, Vol. 53, 123-143, doi:10.1016/j.jmapro.2020.02.013

[6] Altıparmak, S. C.; Yardley, V. A.; Shi, Z.; Lin, J. (2021). Challenges in additive manufacturing of high-strength aluminium alloys and current developments in hybrid additive manufacturing, *International Journal of Lightweight Materials and Manufacture*, Vol. 4, No. 2, 246-261, doi:10.1016/j.ijlmm.2020.12.004

[7] Grguraš, D.; Kern, M.; Pušavec, F. (2019). Cutting performance of solid ceramic and carbide end milling tools in machining of nickel based alloy Inconel 718 and stainless steel 316L, *Advances in Production Engineering & Management*, Vol. 14, No. 1, 27-38, doi:10.14743/apem2019.1.309

[8] Periane, S.; Duchosal, A.; Vaudreuil, S.; Chibane, H.; Morandeau, A.; Xavior, M. A.; Leroy, R. (2020). Selection of machining condition on surface integrity of additive and conventional Inconel 718, *Procedia CIRP*, Vol. 87, 333-338, doi:10.1016/j.procir.2020.02.092

[9] Ji, H.; Gupta, M. K.; Song, Q.; Cai, W.; Zheng, T.; Zhao, Y.; Liu, Z.; Pimenov, D. Y. (2021). Microstructure and machinability evaluation in micro milling of selective laser melted Inconel 718 alloy, *Journal of Materials Research and Technology*, Vol. 14, 348-362, doi:10.1016/j.jmrt.2021.06.081

[10] Fei, J.; Liu, G.; Patel, K.; Özel, T. (2020). Effects of machining parameters on finishing additively manufactured nickel-based alloy Inconel 625, *Journal of Manufacturing and Materials Processing*, Vol. 4, No. 2, Paper 32, 23 pages, doi:10.3390/jmmp4020032

[11] Zhang, H.; Dang, J.; Ming, W.; Xu, X.; Chen, M.; An, Q. (2020). Cutting responses of additive manufactured Ti6Al4V with solid ceramic tool under dry high-speed milling processes, *Ceramics International*, Vol. 46, No. 10, Part A, 14536-14547, doi:10.1016/j.ceramint.2020.02.253

[12] Savković, B.; Kovač, P.; Stoić, A.; Dudić, B. (2020). Optimization of machining parameters using the Taguchi and ANOVA analysis in the face milling of aluminum alloys Al7075, *Technical Gazette*, Vol. 27, No. 4, 1221-1228, doi:10.17559/TV-20190621105149

[13] Ming, W.; Chen, J.; An, Q.; Chen, M. (2019). Dynamic mechanical properties and machinability characteristics of selective laser melted and forged Ti6Al4V, *Journal of Materials Processing Technology*, Vol. 271, 284-292, doi:10.1016/j.jmatprotec.2019.04.015

[14] Li, Z. Z.; Zheng, M.; Zheng, L.; Wu, Z. J.; Liu, D. C. (2003). A solid model-based milling process simulation and optimization system integrated with CAD/CAM, *Journal of Materials Processing Technology*, Vol. 138, No. 1-3, 513-517, doi:10.1016/S0924-0136(03)00137-7

[15] Lee, P.; Altintaş, Y. (1996). Prediction of ball-end milling forces from orthogonal cutting data, *International Journal of Machine Tools and Manufacture*, Vol. 36, No. 9, 1059-1072, doi:10.1016/0890-6955(95)00081-X

[16] Sai, L.; Belguith, R.; Baili, M.; Dessein, G.; Bouzid, W. (2018). An approach to modeling the chip thickness and cutter workpiece engagement region in 3 and 5 axis ball end milling, *Journal of Manufacturing Processes*, Vol. 34, Part A, 7-17, doi:10.1016/j.jmapro.2018.05.018

[17] Guo, M.; Wei, Z.; Wang, M.; Li, S.; Liu, S. (2018). An identification model of cutting force coefficients for five-axis ball-end milling, *The International Journal of Advanced Manufacturing Technology*, Vol. 99, No. 1-4, 937-949, doi:10.1007/s00170-018-2451-6

[18] Hoon Ko, J.; Cho, D.-W. (2005). 3D ball-end milling force model using instantaneous cutting force coefficients, *Journal of Manufacturing Science and Engineering*, Vol. 127, No. 1, 1-12, doi:10.1115/1.1826077

[19] Feng, H.-Y.; Su, N. (2001). A mechanistic cutting force model for 3D ball-end milling, *Journal of Manufacturing Science and Engineering*, Vol. 123, No. 1, 23-29, doi:10.1115/1.1334864

[20] Li, J.; Kilic, Z. M.; Altintas, Y. (2020). General cutting dynamics model for five-axis ball-end milling operations, *Journal of Manufacturing Science and Engineering*, Vol. 142, No. 12, Paper 121003, 13 pages, doi:10.1115/1.4047625

[21] Lee, P.; Altintaş, Y. (1996). Prediction of ball-end milling forces from orthogonal cutting data, *International Journal of Machine Tools and Manufacture*, Vol. 36, No. 9, 1059-1072, doi:10.1016/0890-6955(95)00081-X

[22] Wojciechowski, S.; Maruda, R. W.; Nieslony, P.; Krolczyk, G. M. (2016). Investigation on the edge forces in ball end milling of inclined surfaces, *International Journal of Mechanical Sciences*, Vol. 119, 360-369, doi:10.1016/j.ijmecsci.2016.10.034

[23] Wang, S. B.; Geng, L.; Zhang, Y. F.; Liu, K.; Ng, T. E. (2015). Cutting force prediction for five-axis ball-end milling considering cutter vibrations and run-out, *International Journal of Mechanical Sciences*, Vol. 96-97, 206-215, doi:10.1016/j.ijmecsci.2015.04.007

[24] Kang, W. T.; Derani, M. N.; Ratnam, M. M. (2020). Effect of vibration on surface roughness in finish turning: simulation study, *International Journal of Simulation Modelling*, Vol. 19, No. 4, 595-606, doi:10.2507/IJSIMM19-4-531
[25] Mou, W.; Zhu, S.; Zhu, M.; Han, L.; Jiang, L. (2020). A prediction model of cutting force about ball end milling for sculptured surface, *Mathematical Problems in Engineering*, Vol. 2020, Paper 1389718, 15 pages, doi:10.1155/2020/1389718
[26] Jia, Z.-Y.; Ge, J.; Ma, J.-W.; Gao, Y.-Y.; Liu, Z. (2016). A new cutting force prediction method in ball-end milling based on material properties for difficult-to-machine materials, *The International Journal of Advanced Manufacturing Technology*, Vol. 86, No. 9-12, 2807-2822, doi:10.1007/s00170-016-8351-8
[27] Yang, L.; Zheng, M. L. (2017). Simulation and analysis of ball-end milling of panel moulds based on Deform 3D, *International Journal of Simulation Modelling*, Vol. 16, No. 2, 343-356, doi:10.2507/IJSIMM16(2)CO9
[28] Omar, O. E. E. K.; El-Wardany, T.; Ng, E.; Elbestawi, M. A. (2007). An improved cutting force and surface topography prediction model in end milling, *International Journal of Machine Tools and Manufacture*, Vol. 47, No. 7-8, 1263-1275, doi:10.1016/j.ijmachtools.2006.08.021
[29] Wang, W.; Zhang, W.; Huang, D.; Wang, W. (2021). Cutting force modeling and experimental validation for micro end milling, *The International Journal of Advanced Manufacturing Technology*, Vol. 117, No. 3-4, 933-947, doi:10.1007/s00170-021-07815-8
[30] Vukelic, D.; Kanovic, Z.; Sokac, M.; Santosi, Z.; Budak, I.; Tadic, B. (2021). Modelling of micro-turning process based on constant cutting force, *International Journal of Simulation Modelling*, Vol. 20, No. 1, 146-157, doi:10.2507/IJSIMM20-1-553
[31] Karpat, Y.; Polat, N. (2013). Mechanistic force modeling for milling of carbon fiber reinforced polymers with double helix tools, *CIRP Annals*, Vol. 62, No. 1, 95-98, doi:10.1016/j.cirp.2013.03.105
[32] Kalla, D.; Sheikh-Ahmad, J.; Twomey, J. (2010). Prediction of cutting forces in helical end milling fiber reinforced polymers, *International Journal of Machine Tools and Manufacture*, Vol. 50, No. 10, 882-891, doi:10.1016/j.ijmachtools.2010.06.005
[33] He, Y.; Qing, H.; Zhang, S.; Wang, D.; Zhu, S. (2017). The cutting force and defect analysis in milling of carbon fiber-reinforced polymer (CFRP) composite, *The International Journal of Advanced Manufacturing Technology*, Vol. 93, No. 5-8, 1829-1842, doi:10.1007/s00170-017-0613-6
[34] Wang, F.; Li, Y.; Zhang, B.; Deng, J.; Lin, Y.; Yang, L.; Fu, R. (2022). Theoretical model of instantaneous milling force for CFRP milling with a ball-end milling cutter: Considering spatial dimension and temporal dimension discontinuity effects, *Journal of Manufacturing Processes*, Vol. 75, 346-362, doi:10.1016/j.jmapro.2022.01.021
[35] Gao, H. N.; Shen, D. H.; Yu, L.; Zhang, W. C. (2020). Identification of cutting chatter through deep learning and classification, *International Journal of Simulation Modelling*, Vol. 19, No. 4, 667-677, doi:10.2507/IJSIMM19-4-CO16